Laser-polarization-dependent spontaneous emission of the zero phonon line from single nitrogen–vacancy center in diamond*

Zhang Duo(张 多)[a)†], Li Jia-Hua(李家华)[b)c)‡], and Yang Xiao-Xue(杨晓雪)[b)]

[a)] School of Electrical and Electronic Engineering, Wuhan Polytechnic University, Wuhan 430023, China
[b)] School of Physics, Huazhong University of Science and Technology, Wuhan 430074, China
[c)] Key Laboratory of Fundamental Physical Quantities Measurement of Ministry of Education, Wuhan 430074, China

(Received 22 July 2013; revised manuscript received 8 September 2013; published online 10 February 2014)

We investigate spontaneous emission properties and control of the zero phonon line (ZPL) from a diamond nitrogen–vacancy (NV) center coherently driven by a single elliptically polarized control field. We use the Schrödinger equation to calculate the probability amplitudes of the wave function of the coupled system and derive analytical expressions of the spontaneous emission spectra. The numerical results show that a few interesting phenomena such as enhancement, narrowing, suppression, and quenching of the ZPL spontaneous emission can be realized by modulating the polarization-dependent phase, the Zeeman shift, and the intensity of the control field in our system. In the dressed-state picture of the control field, we find that multiple spontaneously generated coherence arises due to three close-lying states decaying to the same state. These results are useful in real experiments.

Keywords: diamond nitrogen–vacancy center, spontaneous emission, quantum interference

PACS: 42.50.Gy, 32.80.Qk, 32.50.+d, 76.30.Mi **DOI:** 10.1088/1674-1056/23/4/044204

1. Introduction

Spontaneous emission in atomic systems, is recognized as one of the best-known fundamental processes based on the interaction of atomic systems with the environmental modes. In the past few years, modification and control of the spontaneous emission have attracted much attention because of its potential applications in lasing without inversion (LWI),[1–5] transparent high-index materials,[6–9] high-precision spectroscopy and magnetometry,[10–12] quantum information and computing,[13–15] etc. There are two main mechanisms to control the spontaneous emission of atoms. In the first mechanism, the spontaneous emission of a multilevel atomic system can be modified just by putting atoms into different environments,[16–26] such as in free space, in optical waveguides, in photonic crystal (PC) materials, and in optical cavities, which have different densities of electromagnetic modes. On the other hand, in the second mechanism, the manipulation of spontaneous emission can be achieved by using external coherent fields to couple atoms.[27–33]

In recent years, the nitrogen–vacancy (NV) center in diamond nanocrystal has emerged as a particularly strong candidate for solid-state quantum physics experiments and quantum information processing because it possesses a long electronic spin decoherence time at room temperature.[34–47] Owing to the potential applications of NV center in quantum information and quantum computing, many properties and interesting phenomena about NV center are researched and discussed recently. Santori *et al.*[48] demonstrated coherent population trapping in a single NV center in diamond under optical excitation, the results show that all-optical control of a single spin is possible in diamond. Yang *et al.*[49,50] investigated quantum state transfer and quantum correlation in a composite system consisting of two NV centers embedded in two spatially separated single-mode nanocavities in a planar photonic crystal, and analyzed the relevant entanglement dynamics in the presence of decoherence and the non-Markovian dynamics of quantum correlation between two initially entangled NV centers. Wang *et al.*[51] studied the applicability of the time-optimal bang–bang control designed for spin $1/2$ to the rotation of the electron spin of an NV center in diamond. They found that the bang–bang control protocol decreases the rotation time by 20%–25% in comparison with the traditional oscillating sinusoidal driving.

Unfortunately, it is difficult to achieve remarkable and ideal optical properties of the diamond NV centers because of the small Debye–Waller (DW) factor. Specifically, for the NV centers, even at cryogenic temperatures only a small fraction of about 3%–4% of the radiation can be emitted into the Fourier-limited zero phonon line (ZPL), and most of the light is emitted at much larger wavelengths (600 nm–800 nm, the so-called phononic or vibronic sideband).[47,52] In order to overcome the above obstacle, based on the second mechanism mentioned above (i.e., laser-induced atomic coherence and quantum interference), here we put forward a scheme to

*Part of this project supported by the National Natural Science Foundation of China (Grant Nos. 11375067, 11275074, 11104210, 11004069, and 91021011), the Doctoral Foundation of the Ministry of Education of China (Grant No. 20100142120081), and the National Basic Research Program of China (Grant No. 2012CB922103).

†Corresponding author. E-mail: zhangduo10@gmail.com
‡Corresponding author. E-mail: huajia_li@163.com

© 2014 Chinese Physical Society and IOP Publishing Ltd

explore the spontaneous emission properties and optical control of the ZPL from a nanodiamond NV center coupled by a single elliptically polarized control field with different ellipticities. It is found that the spectral-line enhancement, narrowing, suppression, and quenching of the ZPL spontaneous emission can be realized by modulating the polarization-dependent phase, the Zeeman shift or the external magnetic field, and the intensity of the control field in our system. Our proposed system is similar to atomic vapors in the energy level structure, but our work is very different from previous atomic systems. First of all, our numerical results for spontaneous emission of the NV center are easily experimentally observed because of their long electronic spin decoherence time, not as the atomic gas which has to decrease the temperature to several tens of μK in order to eliminate the Doppler broadening effect. Thus this relaxes the bandwidth and decoherence constraints of NV systems. Secondly, our study of controlling the diamond NV center with a laser field and a magnetic field is more convenient than controlling atomic gas experimentally due to the solid state of the NV center. Thirdly, we only need one single elliptically polarized control field to couple two electric dipole transitions simultaneously and the polarization-dependent phase difference between the two circularly polarized components of the control field can be used to control spontaneous emission effectively.

The paper is organized as follows. In Section 2, we establish the physical model and its theoretical description. By solving the coupled amplitude equations of motion for a tripod-type NV center, we derive explicit analytical expressions of the spontaneous emission spectra. In Section 3, we analyze our results and discuss in detail the influence of the polarization-dependent phase of two components of an elliptically polarized laser field, the intensity of the external magnetic field and the control field, and the initial probability amplitudes on the spontaneous emission spectra. In Section 4, we introduce the dressed-state description of the control fields to explain the properties of spontaneous emission spectra. In Section 5, we discuss the possible experimental realization. Finally, our main conclusions are summarized in Section 6.

2. Description of the model and equation

We consider strained nanodiamond NV centers coupled by a single elliptically polarized laser as shown in Fig. 1(a). The NV center is a point defect in the diamond lattice, which consists of a substitutional nitrogen atom (N) plus a vacancy (V) in an adjacent lattice site. The NV center we described in this paper is negatively charged with two unpaired electrons located at the vacancy, usually treated as electron spin-1.[53] As a result, the spin–spin interaction leads to the energy splitting $D_{\rm gs} = 2.88$ GHz between $|^3A, m_s = 0\rangle$ and $|^3A, m_s = \pm 1\rangle$. Meanwhile, the degeneracy of the levels $|^3A, m_s = \pm 1\rangle$ can be lifted by employing an external magnetic field B along the quantized symmetry axis of the NV center, which induces a level splitting $2\Delta_B$. We label $|^3A, m_s = 0\rangle$, $|^3A, m_s = -1\rangle$, and $|^3A, m_s = +1\rangle$ as $|4\rangle$, $|1\rangle$, and $|2\rangle$, respectively. The NV center has a relatively complicated structure of excited states,[44] which includes six excited states defined by the method of group theory as

$$
\begin{aligned}
|A_1\rangle &= \frac{1}{\sqrt{2}}(|E_-, m_s = +1\rangle - |E_+, m_s = -1\rangle),\\
|A_2\rangle &= \frac{1}{\sqrt{2}}(|E_-, m_s = +1\rangle + |E_+, m_s = -1\rangle),\\
|E_x\rangle &= |X, m_s = 0\rangle, \quad |E_y\rangle = |Y, m_s = 0\rangle,\\
|E_1\rangle &= \frac{1}{\sqrt{2}}(|E_-, m_s = -1\rangle - |E_+, m_s = +1\rangle),
\end{aligned}
$$

and

$$
|E_2\rangle = \frac{1}{\sqrt{2}}(|E_-, m_s = -1\rangle + |E_+, m_s = +1\rangle),
$$

with $|E_+\rangle$, $|E_-\rangle$ being orbital states with angular momentum projection ± 1 along the NV axis, and $|X\rangle$, $|Y\rangle$ being orbital states with zero projection of angular momentum. Under external strain, the excited states can be splitting and mixed,[47] the state $|3\rangle$ can be considered as a mixed state of two excited states

$$
|A_2\rangle = \frac{1}{\sqrt{2}}(|E_-, m_s = +1\rangle + |E_+, m_s = -1\rangle),
$$

and $|E_x\rangle = |X, m_s = 0\rangle$, i.e., $|3\rangle = \alpha|A_2\rangle + \beta|E_x\rangle$ with $|\alpha|^2 + |\beta|^2 = 1$. The state $|3\rangle$ decays to the ground-state sublevels $|1\rangle$ and $|2\rangle$ with radiation of σ^+ and σ^- circular polarizations, respectively. An elliptically polarized control field with a carrier frequency $\omega_{\rm c}$ and a wave vector $k_{\rm c}$ can be regarded as a combination of the right- and left-circularly polarized components, which can be used to create electric dipole transitions between the excited state $|3\rangle$ and the ground states $|1\rangle$ and $|2\rangle$ simultaneously. The elliptically polarized control field can be obtained by using a quarter-wave plate.[54] An initial vertically polarized control beam with intensity I_0 and electric field amplitude $E_0 = \sqrt{2I_0/\varepsilon_0 c}$, where ε_0 is the permittivity of free space and c is the speed of light, becomes elliptically polarized after passing through the quarter-wave plate that has been rotated by an angle θ (the polarization-dependent parameter), so the polarized control beam can be decomposed into $E_{\rm c} = E^+\sigma^+ + E^-\sigma^-$, where

$$
E^+ = \frac{E_0}{\sqrt{2}}(\cos\theta + \sin\theta)\mathrm{e}^{\mathrm{i}\theta}
$$

and

$$
E^- = \frac{E_0}{\sqrt{2}}(\cos\theta - \sin\theta)\mathrm{e}^{-\mathrm{i}\theta}.
$$

Here, σ^+ and σ^- are the unit vectors of the right- and left-circularly polarized bases, respectively. When $\theta = 0$ and $\pi/2$, we have $E^+ = E^-$, that is, the control beam is linearly polarized. When $\theta = \pi/4$ ($3\pi/4$), we have $E^- = 0$ ($E^+ = 0$),

that is, the control beam is right-circularly (left-circularly) polarized. A quarter-wave plate can change the strength and phase difference of the two electric field components. Then, Rabi frequencies become $2\Omega_{c+} = -\mu_{31}E^{+}/\hbar = 2\Omega_c(\cos\theta + \sin\theta)e^{i\theta}$ and $2\Omega_{c-} = -\mu_{32}E^{-}/\hbar = 2\Omega_c(\cos\theta - \sin\theta)e^{-i\theta}$, here we assume $\mu_{31} = \mu_{32} = \mu$ (μ denotes the electric dipole moment between the corresponding transitions) and $\Omega_c = -\mu E_0/(2\sqrt{2}\hbar)$. While the transition from state $|3\rangle$ to state $|4\rangle$ is assumed to be coupled by vacuum modes in the free space. It should be pointed out that the dipole–dipole interaction between the nitrogen and the vacancy has been neglected because we consider a single NV center in diamond. Recently it has been found that the dipole–dipole interaction between nanoparticles plays a very important role in nanocrystals and nanowires.[55]

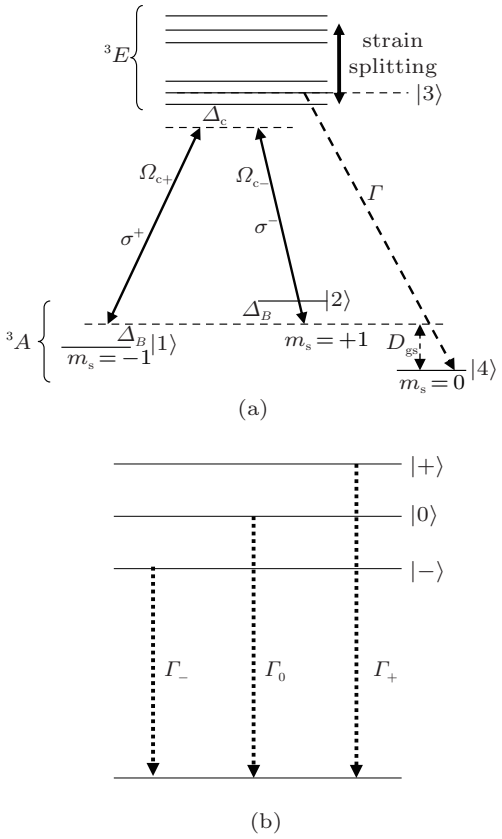


Fig. 1. (a) A schematic diagram of an NV center interacting with an elliptically polarized field. A right(left)-hand circularly polarized component $\Omega_{c+}(\Omega_{c-})$ of the elliptically polarized control field induces the transitions $|3\rangle \leftrightarrow |1\rangle$ ($|3\rangle \leftrightarrow |2\rangle$). The state $|3\rangle$ can be considered as a mixed state of two excited states $|A_2\rangle = (|E_-, m_s = +1\rangle + |E_+, m_s = -1\rangle)/\sqrt{2}$ and $|E_x\rangle = |X, m_s = 0\rangle$ under strain, $|^3A, m_s = 0\rangle$, $|^3A, m_s = -1\rangle$, and $|^3A, m_s = +1\rangle$ are labelled as $|4\rangle$, $|1\rangle$, and $|2\rangle$, respectively. The symbol Δ_c is the frequency detunings of the control field, see the text for details. By applying a uniform magnetic field along the quantized symmetry axis of the NV center, the degeneracy among the ground states $|1\rangle$ and $|2\rangle$ is lifted, where an amount Δ_B stands for the Zeeman shift. $D_{gs} = 2.88$ GHz is the zero-field splitting between the ground state sublevels $|^3A, m_s = 0\rangle$ and $|^3A, m_s = \pm 1\rangle$ ($|^3A, m_s = \pm 1\rangle$ are degenerate at zero magnetic field) of the NV center. (b) A corresponding dressed-state description of the elliptically polarized control field.

Under the rotating-wave approximation (RWA) and electric-dipole approximation (EDA), the interaction Hamiltonian for the system composed of the NV center, control fields, and vacuum modes can be written as[56–58] (see Appendix A for details)

$$\hat{H}_I = 2\Delta_B|2\rangle\langle 2| + (\Delta_B + \Delta_c)|3\rangle\langle 3| + \Big[\Omega_{c+}|3\rangle\langle 1| + \Omega_{c-}|3\rangle\langle 2| + \sum_k g_k b_k e^{-i(\Delta_B+\Delta_c-\delta_k)t}|3\rangle\langle 4| + \text{H.c.}\Big], \quad (1)$$

where H.c. means Hermitian conjugation, the notation $\Delta_c = \omega_{31} - \Delta_B - \omega_c = \omega_{32} + \Delta_B - \omega_c$ is the detuning of the transitions from the corresponding laser frequencies (see Fig. 1(a)), where $\omega_{31} = (E_3 - E_1)/\hbar$ ($\omega_{32} = (E_3 - E_2)/\hbar$) is the transition frequency between the energy levels $|3\rangle$ and $|1\rangle$ ($|2\rangle$). Δ_B is the Zeeman shift of levels $|1\rangle$ and $|2\rangle$ in the presence of the magnetic field. ($b_k^\dagger$) b_k is the creation (annihilation) operator for the k-th vacuum mode with frequency ω_k. $\delta_k = \omega_{34} - \omega_k$ and g_k denote the detuning and the coupling constant between the k-th vacuum mode and the resonance $|3\rangle \to |4\rangle$.

The wave function of the NV center system, at a specific time t, can be expanded in terms of the bare-state eigenvectors such that

$$|\Psi(t)\rangle = [a_1(t)|1\rangle + a_2(t)|2\rangle + a_3(t)|3\rangle]\{0\} + \sum_k a_k(t)|4\rangle|1_k\rangle, \quad (2)$$

where $a_j(t)$ ($j = k, 1$–3) stands for the time-dependent probability amplitude of the NV center. $\{0\}$ represents the absence of photons in all the vacuum modes, and $|1_k\rangle$ indicates that there is one photon in the k-th vacuum mode.

Similar to the method used in three-level quantum dots (QDs),[59,60] we make use of the well-known Schrödinger equation in the interaction picture $i\partial|\Psi(t)\rangle/\partial t = \hat{H}_I|\Psi(t)\rangle$, the coupled equations of motion for the probability amplitude evolution of the NV center's wave functions can be readily obtained as

$$\frac{\partial a_1(t)}{\partial t} = -i\Omega_{c+}^* a_3(t), \quad (3)$$

$$\frac{\partial a_2(t)}{\partial t} = -i2\Delta_B a_2(t) - i\Omega_{c-}^* a_3(t), \quad (4)$$

$$\frac{\partial a_3(t)}{\partial t} = -i\left(\Delta_B + \Delta_c - i\frac{\Gamma}{2}\right)a_3(t) - i\Omega_{c+}a_1(t) - i\Omega_{c-}a_2(t), \quad (5)$$

$$\frac{\partial a_k(t)}{\partial t} = -ig_k^* e^{i(\Delta_B+\Delta_c-\delta_k)t}a_3(t), \quad (6)$$

where $\Gamma = 2\pi|g_k|^2 D(\omega_k)$ is the spontaneous-decay rate from level $|3\rangle$ to level $|4\rangle$, and $D(\omega_k)$ is the vacuum-mode density at frequency ω_k in the free space.

Carrying out the Laplace transformations

$$\tilde{a}_j(s) = \int_0^\infty e^{-st} a_j(t)\,dt,$$

where s is the time Laplace transform variable for Eqs. (3)–(5) and integrating Eq. (6) with respect to t', we have the probability amplitude

$$\begin{aligned}\tilde{a}_3(s) = {} & [-\mathrm{i}(s+2\mathrm{i}\Delta_B)\Omega_{\mathrm{c}+}a_1(0) - \mathrm{i}s\Omega_{\mathrm{c}-}a_2(0) \\ & + s(s+2\mathrm{i}\Delta_B)a_3(0)]\Big/\Big\{s(s+2\mathrm{i}\Delta_B) \\ & \times \left[s+\mathrm{i}\left(\Delta_B+\Delta_{\mathrm{c}}-\mathrm{i}\frac{\Gamma}{2}\right)\right] + (s+2\mathrm{i}\Delta_B)|\Omega_{\mathrm{c}+}|^2 \\ & + s|\Omega_{\mathrm{c}-}|^2\Big\}, \end{aligned} \tag{7}$$

where $a_j(0)$ ($j = 1$–3) is the probability amplitude at the initial time $t = 0$.

The spontaneous emission spectra of the ZPL are the Fourier transform of $\langle E^-(t+\tau)E^+(t)\rangle_{t\to\infty}$, and can be written as

$$S(\delta_k) = \frac{\Gamma}{2\pi|g_k|^2}|a_k(t\to\infty)|^2$$

for our studied NV center system. According to the above equation, we have

$$\begin{aligned} a_k(t\to\infty) &= -\mathrm{i}g_k^*\int_0^\infty \mathrm{e}^{\mathrm{i}(\Delta_B+\Delta_{\mathrm{c}}-\delta_k)t'}a_3(t')\,\mathrm{d}t' \\ &= -\mathrm{i}g_k^*\tilde{a}_3(s=-\mathrm{i}(\Delta_B+\Delta_{\mathrm{c}}-\delta_k)). \end{aligned}$$

Substituting the expression (7) of $\tilde{a}_3(s)$ into the expression of $a_k(t\to\infty)$, we can obtain

$$\begin{aligned} & S(\delta_k) \\ &= \frac{\Gamma}{2\pi|g_k|^2}|a_k(t\to\infty)|^2 \\ &= \frac{\Gamma}{2\pi}|\tilde{a}_3(s=-\mathrm{i}(\Delta_B+\Delta_{\mathrm{c}}-\delta_k))|^2 \\ &= \frac{\Gamma}{2\pi}\left|\frac{a_3(0)-\dfrac{\Omega_{\mathrm{c}+}}{\delta_k-\Delta_B-\Delta_{\mathrm{c}}}a_1(0)-\dfrac{\Omega_{\mathrm{c}-}}{\delta_k+\Delta_B-\Delta_{\mathrm{c}}}a_2(0)}{\left(\mathrm{i}\delta_k+\dfrac{\Gamma}{2}\right)+\dfrac{|\Omega_{\mathrm{c}+}|^2}{\mathrm{i}(\delta_k-\Delta_B-\Delta_{\mathrm{c}})}+\dfrac{|\Omega_{\mathrm{c}-}|^2}{\mathrm{i}(\delta_k+\Delta_B-\Delta_{\mathrm{c}})}}\right|^2, \end{aligned} \tag{8}$$

where Eq. (8) is the main result of the present study. Specifically, we display the four different cases as listed below.

Case i Under the conditions $a_3(0) = 1$ and $a_1(0) = a_2(0) = 0$, so that the ZPL spontaneous emission spectra $S(\delta_k)$ in Eq. (8) can be explicitly expressed in the following form

$$S(\delta_k) = \frac{\Gamma}{2\pi}\frac{1}{\left|\left(\mathrm{i}\delta_k+\dfrac{\Gamma}{2}\right)+\dfrac{|\Omega_{\mathrm{c}}|^2(1+\sin 2\theta)}{\mathrm{i}(\delta_k-\Delta_B-\Delta_{\mathrm{c}})}+\dfrac{|\Omega_{\mathrm{c}}|^2(1-\sin 2\theta)}{\mathrm{i}(\delta_k+\Delta_B-\Delta_{\mathrm{c}})}\right|^2}. \tag{9}$$

Case ii Under the conditions $a_1(0) = 1$ and $a_3(0) = a_2(0) = 0$, we have the result

$$S(\delta_k) = \frac{\Gamma}{2\pi}\left|\frac{\Omega_{\mathrm{c}}(\cos\theta+\sin\theta)}{(\delta_k-\Delta_B-\Delta_{\mathrm{c}})\left[\left(\mathrm{i}\delta_k+\dfrac{\Gamma}{2}\right)+\dfrac{|\Omega_{\mathrm{c}}|^2(1+\sin 2\theta)}{\mathrm{i}(\delta_k-\Delta_B-\Delta_{\mathrm{c}})}+\dfrac{|\Omega_{\mathrm{c}}|^2(1-\sin 2\theta)}{\mathrm{i}(\delta_k+\Delta_B-\Delta_{\mathrm{c}})}\right]}\right|^2. \tag{10}$$

Case iii Under the conditions $a_2(0) = 1$ and $a_3(0) = a_1(0) = 0$, we have the result

$$S(\delta_k) = \frac{\Gamma}{2\pi}\left|\frac{\Omega_{\mathrm{c}}(\cos\theta-\sin\theta)}{(\delta_k+\Delta_B-\Delta_{\mathrm{c}})\left[\left(\mathrm{i}\delta_k+\dfrac{\Gamma}{2}\right)+\dfrac{|\Omega_{\mathrm{c}}|^2(1+\sin 2\theta)}{\mathrm{i}(\delta_k-\Delta_B-\Delta_{\mathrm{c}})}+\dfrac{|\Omega_{\mathrm{c}}|^2(1-\sin 2\theta)}{\mathrm{i}(\delta_k+\Delta_B-\Delta_{\mathrm{c}})}\right]}\right|^2. \tag{11}$$

Case iv Under the conditions $a_1(0) = a_2(0) = 1/\sqrt{2}$ and $a_3(0) = 0$, we have the result

$$S(\delta_k) = \frac{\Gamma}{2\pi}\left|\frac{\dfrac{\Omega_{\mathrm{c}}(\cos\theta+\sin\theta)\mathrm{e}^{\mathrm{i}\theta}}{\sqrt{2}(\delta_k-\Delta_B-\Delta_{\mathrm{c}})}+\dfrac{\Omega_{\mathrm{c}}(\cos\theta-\sin\theta)\mathrm{e}^{-\mathrm{i}\theta}}{\sqrt{2}(\delta_k+\Delta_B-\Delta_{\mathrm{c}})}}{\left(\mathrm{i}\delta_k+\dfrac{\Gamma}{2}\right)+\dfrac{|\Omega_{\mathrm{c}}|^2(1+\sin 2\theta)}{\mathrm{i}(\delta_k-\Delta_B-\Delta_{\mathrm{c}})}+\dfrac{|\Omega_{\mathrm{c}}|^2(1-\sin 2\theta)}{\mathrm{i}(\delta_k+\Delta_B-\Delta_{\mathrm{c}})}}\right|^2. \tag{12}$$

It is not difficult to find from Eqs. (9)–(12) that the analytical expressions for the zero phonon line spontaneous emission spectra $S(\delta_k)$ is sensitively dependent on the controllable parameters of the system such as the polarization-dependent parameter θ, the Zeeman shift Δ_B or the magnetic field intensity B ($\Delta_B \propto B$), the detuning Δ_{c}, and the intensity Ω_{c} of the control field. As a consequence, we can control the zero phonon line spontaneous emission of the nanodiamond nitrogen–vacancy center by adjusting these system parameters under proper conditions.

3. Results and discussion

In this section, we present a few numerical results about the ZPL spontaneous emission spectra $S(\delta_k)$. All parameters used in the following calculations are scaled by γ, which should be in the order of MHz for the diamond NV center. First of all, we will analyze how the polarization-dependent phase difference θ between the two circularly polarized components of the control beam modifies the ZPL spontaneous emission via the numerical calculations based on Eq. (8). In Fig. 2, we plot the spontaneous emission spectra $S(\delta_k)$ versus the detuning δ_k for different phase differences under the condition of $a_3(0) = 1$ and $a_1(0) = a_2(0) = 0$. The insets display 10 typical forms of polarized control beam. The initial state preparation can be achieved by optical pumping in experiment.[48] When $\theta = 0$ [see Fig. 2(a)], we have the result $E^+ = E^-$, that is, the control beam is linearly polarized and the intensity of the right-circularly polarized component is the same with the left-circularly polarized component. The ZPL spontaneous emission spectra exhibit a central ultranarrow line and two wider sideband lines with two fluorescence-quenching points. It can be easily seen from Eq. (9) that when $\delta_k = \Delta_B + \Delta_c$ or $\Delta_c - \Delta_B$, the denominator of $S(\delta_k)$ tends to infinity, while the numerator of $S(\delta_k)$ is 1, as a result two fluorescence-quenching points arise. For the case that $\theta = \pi/6$ [see Fig. 2(b)], the control beam is right-handed elliptically polarized and the central ultranarrow line is suppressed obviously. For the case that $\theta = \pi/4$ [see Fig. 2(c)], we have $E^- = 0$; that is, the control beam is right-handed circularly polarized. The central ultranarrow spectral line is completely suppressed, hence we can observe two peaks with a normal width and one fluorescence-quenching point located at $\delta_k = \Delta_B + \Delta_c = 0.6\gamma$. While when phase difference θ increases to $\pi/3$ ($\pi/2$), the ZPL spontaneous emission spectra show the same shape with $\theta = \pi/6$ (0) as shown in Fig. 2(b) [Fig. 2(a)] because the control beam's intensity distributions are the same. When θ further increases to $7\pi/12$ [see Fig. 2(d)], that is to say, the control beam is left-handed elliptically polarized, then the central ultranarrow line appears again and the ZPL spontaneous emission spectra show a three-peak structure. With the increase of θ to $2\pi/3$ [see Fig. 2(e)], the control beam is left-handed elliptically polarized, and the central ultranarrow line can be greatly suppressed again. When θ increases to $3\pi/4$ [see Fig. 2(f)], $E^+ = 0$ and the control beam is left-handed circularly polarized. The central ultranarrow line completely disappears and only one fluorescence-quenching point located at $\delta_k = \Delta_c - \Delta_B = 0.4\gamma$. When phase difference θ increases to $5\pi/6$ ($11\pi/12$), the ZPL spontaneous emission spectra show the same shape as $\theta = 2\pi/3$ ($7\pi/12$) [see Figs. 2(e) and 2(d)].

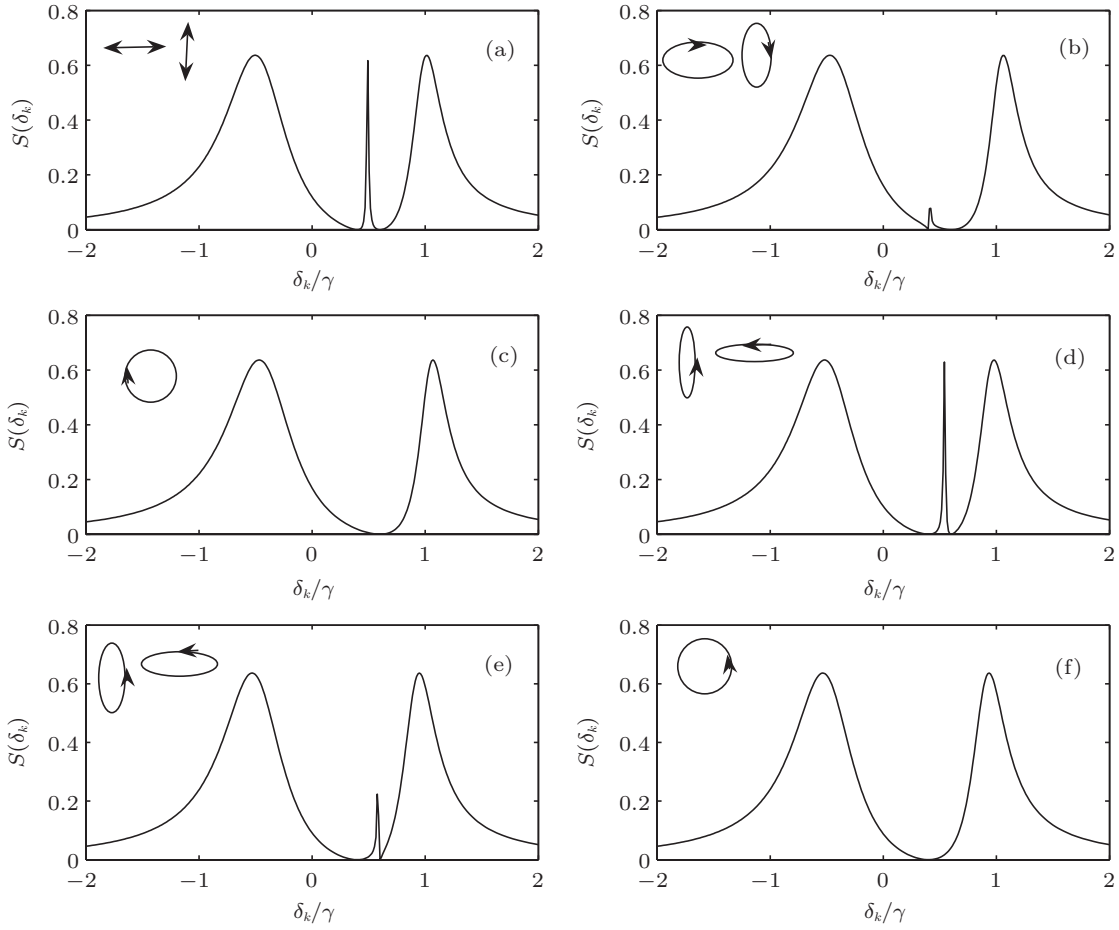


Fig. 2. Spontaneous emission spectra $S(\delta_k)$ (in units of γ^{-1}) for $\Omega_c = 0.5\gamma$, $\Delta_B = 0.1\gamma$, $\Delta_c = 0.5\gamma$, $a_3(0) = 1$, $a_1(0) = a_2(0) = 0$, and $\Gamma = \gamma$. The insets show ten typical forms of polarized control field. (a) $\theta = 0, \pi/2$; (b) $\theta = \pi/6, \pi/3$; (c) $\theta = \pi/4$; (d) $\theta = 7\pi/12, 11\pi/12$; (e) $\theta = 2\pi/3, 5\pi/6$; (f) $\theta = 3\pi/4$.

As can be seen, the analytical solution is in excellent agreement with the numerical calculation. From the above expression (9), we can find that the ZPL spontaneous emission spectra $S(\delta_k)$ is strongly dependent on the laser-polarization-dependent phase θ and also is a periodical function of the relative phase θ with a period π. Furthermore, it can be easily seen from the expression (9) that the relations $[S(\delta_k)]_\theta = [S(\delta_k)]_{\pi/2-\theta} = [S(\delta_k)]_{3\pi/2-\theta}$ hold, which can well explain the numerical results of Fig. 2. The interesting phenomena in the ZPL spontaneous emission spectra discussed above can be qualitatively attributed to multiple spontaneously generated coherence[61–64] among the transitions $|+\rangle \to |4\rangle$, $|0\rangle \to |4\rangle$, and $|-\rangle \to |4\rangle$ [see Fig. 1(b)]. We can see that when populations are initially prepared in level $|3\rangle$, they decay to the ground state $|4\rangle$ through three main processes: $|3\rangle \to |1\rangle \to |3\rangle \to |4\rangle$, $|3\rangle \to |2\rangle \to |3\rangle \to |4\rangle$, and $|3\rangle \to |4\rangle$. Due to quantum interference between three competitive pathways, the spontaneous emission will have two fluorescence-quenching points at $\delta_k = \Delta_c \pm \Delta_B$. While when $\theta = \pi/6$ and $\pi/3$ ($2\pi/3$ and $5\pi/6$), the control beam's intensity distributions are the same, and destructive quantum interferences between pathways $|3\rangle \to |1\rangle \to |3\rangle \to |4\rangle$ and $|3\rangle \to |2\rangle \to |3\rangle \to |4\rangle$ lead to the suppression of the central ultranarrow line. When $\theta = \pi/4$ ($\theta = 3\pi/4$), $E^- = 0$ ($E^+ = 0$) and one of the decay channels $|3\rangle \to |2\rangle \to |3\rangle \to |4\rangle$ ($|3\rangle \to |1\rangle \to |3\rangle \to |4\rangle$) disappears, thus leading to only one fluorescence-quenching point $\delta_k = \Delta_B + \Delta_c$ ($\delta_k = \Delta_c - \Delta_B$).

In what follows, we will analyze how the external magnetic field modifies the ZPL spontaneous emission spectra $S(\delta_k)$ via the numerical calculations based on Eq. (9). In Fig. 3, we plot the ZPL spontaneous emission spectra $S(\delta_k)$ versus the detuning δ_k by modulating the intensity of the external magnetic field under the condition of $a_3(0) = 1$, $a_1(0) = a_2(0) = 0$. For the case that no magnetic field is applied (i.e., $B = 0$ in Fig. 3(a), which corresponds to $\Delta_B = 0$), there is no level splitting between levels $|1\rangle$ and $|2\rangle$. That is to say, $|1\rangle$ and $|2\rangle$ are the same level, the ZPL spontaneous emission spectra display two normal width peaks with one fluorescence-quenching point located at $\delta_k = \Delta_p$. Under the condition of applying the external magnetic field, B corresponds to $\Delta_B = 0.1\gamma$, and as shown in Fig. 3(b), we can see that a low and narrow line emerges in the middle of two wider emission peaks with two fluorescence-quenching points. When the external magnetic field is further increased, a half of the level splitting between levels $|1\rangle$ and $|2\rangle$ $\Delta_B = 0.3\gamma$ [see Fig. 3(c)], the central narrow line is enhanced obviously. In addition, the two fluorescence-quenching points and two wider side emission peaks move away from each other. With further increasing the intensity of the external magnetic field corresponding to Zeeman shift $\Delta_B = 1.5\gamma$ [see Fig. 3(d)], two side peaks evolve into two ultranarrow lines,

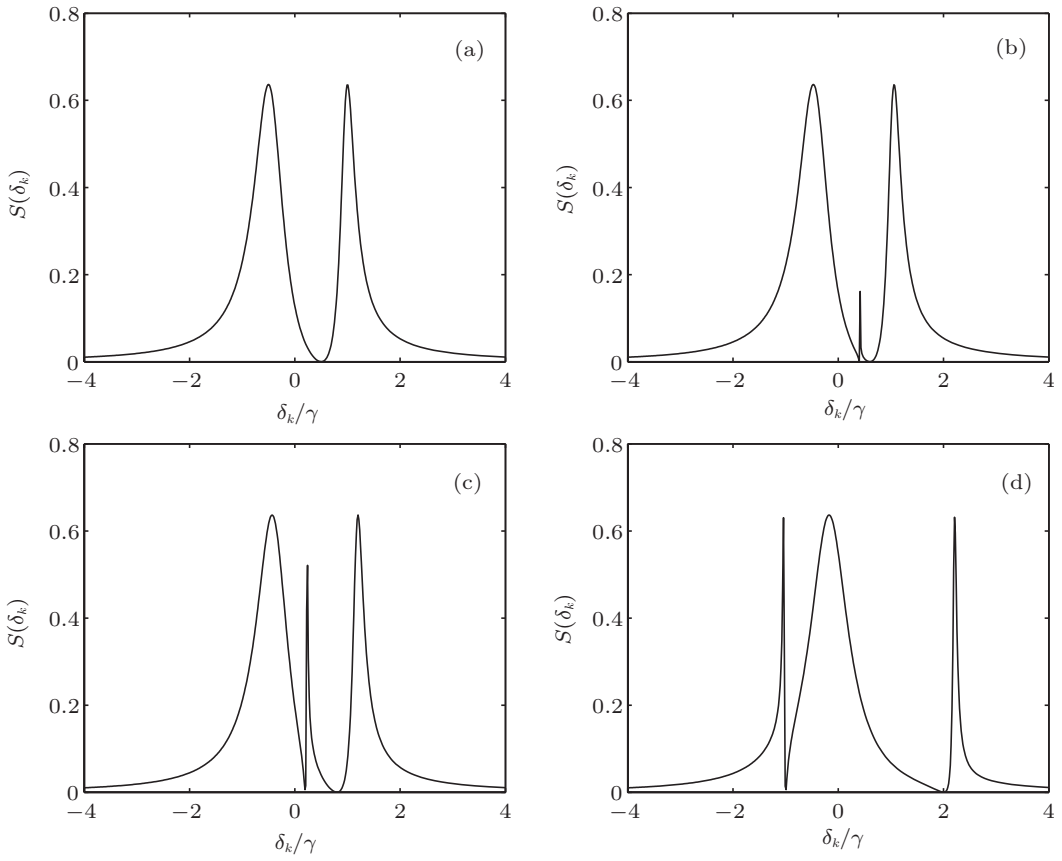


Fig. 3. Spontaneous emission spectra $S(\delta_k)$ (in units of γ^{-1}) for $\Omega_c = 0.5\gamma$, $\Delta_c = 0.5\gamma$, $\theta = \pi/6$, $a_3(0) = 1$, $a_1(0) = a_2(0) = 0$, and $\Gamma = \gamma$. (a) $\Delta_B = 0$; (b) $\Delta_B = 0.1\gamma$; (c) $\Delta_B = 0.3\gamma$; (d) $\Delta_B = 1.5\gamma$.

while the ultranarrow line evolves into a central peak simultaneously. Meanwhile, two fluorescence-quenching points are separated from a short to a long distance. The reason for the above-observed spectral lines can be explained as follows. When $B = 0$, which corresponds to $\Delta_B = 0$, we have the relationship

$$S(\delta_k) \propto \frac{1}{\left|\left(\mathrm{i}\delta_k + \frac{\Gamma}{2}\right) + \frac{2|\Omega_c|^2}{\mathrm{i}(\delta_k - \Delta_c)}\right|^2}.$$

It is only one fluorescence-quenching point that exists in the ZPL spontaneous-emission spectra at $\delta_k = \Delta_c$. At the same time, the two-photon resonance condition is fulfilled, the so-called dark state or coherent population trapping (CPT) state can be formed and an electron is always populated in two lower levels $|1\rangle$ and $|2\rangle$, so spontaneous emission spectra exhibit two peaks. However, when $B \neq 0$ corresponding to $\Delta_B \neq 0$, that is to say, the CPT condition is deviated, we can observe an extra ultranarrow spectral line and two fluorescence-quenching points. The two fluorescence-quenching points exist in the spontaneous-emission spectra at $\delta_k = \Delta_c + \Delta_B$ and $\delta_k = \Delta_c - \Delta_B$, respectively.

In Fig. 4, we also plot the ZPL spontaneous emission spectra $S(\delta_k)$ versus δ_k for four different intensities of the control field under the condition that $\Delta_B = 0.3\gamma$ and keeping other parameters fixed. As can be seen, the change of the control field intensity has not had any effects on the position of the two fluorescence-quenching points but can affect appreciably both the width and separation distance of spectral lines. With a gradual increase of the intensity of the external control field, we can see that the middle peak becomes narrower and lower, while the two sideband peaks go away from each other slowly. For the case that $\Omega_c = 0.2\gamma$ [see Fig. 4(a)], the ZPL spontaneous emission spectra exhibit three peaks with equal height and the left peak is wider than the right two peaks. When the external control field intensity increases to $\Omega_c = 0.5\gamma$ [see Fig. 4(b)], the heights of three peaks have not had any change while the middle peak becomes narrower and the right peak becomes wider. When the external control field intensity further increases to $\Omega_c = 0.8\gamma$ [see Fig. 4(c)], the middle peak evolves to an ultranarrow line and the height becomes lower, while the two side peaks keep away from the cental ultranarrow line. When we continue to increase the external control field intensity to a certain value $\Omega_c = 1.5\gamma$ as shown in Fig. 4(d), the central ultranarrow line is more obvious and the two side peaks are symmetrical about the central ultranarrow line, accompanied by the fact that the separation distance between the two side peaks becomes wider.

In order to further show the influence of the initial probability amplitudes on the ZPL spontaneous emission spectra $S(\delta_k)$, we give the corresponding curves in Fig. 5. The specific results are as follows. For the case that $a_1(0) = 1$ and

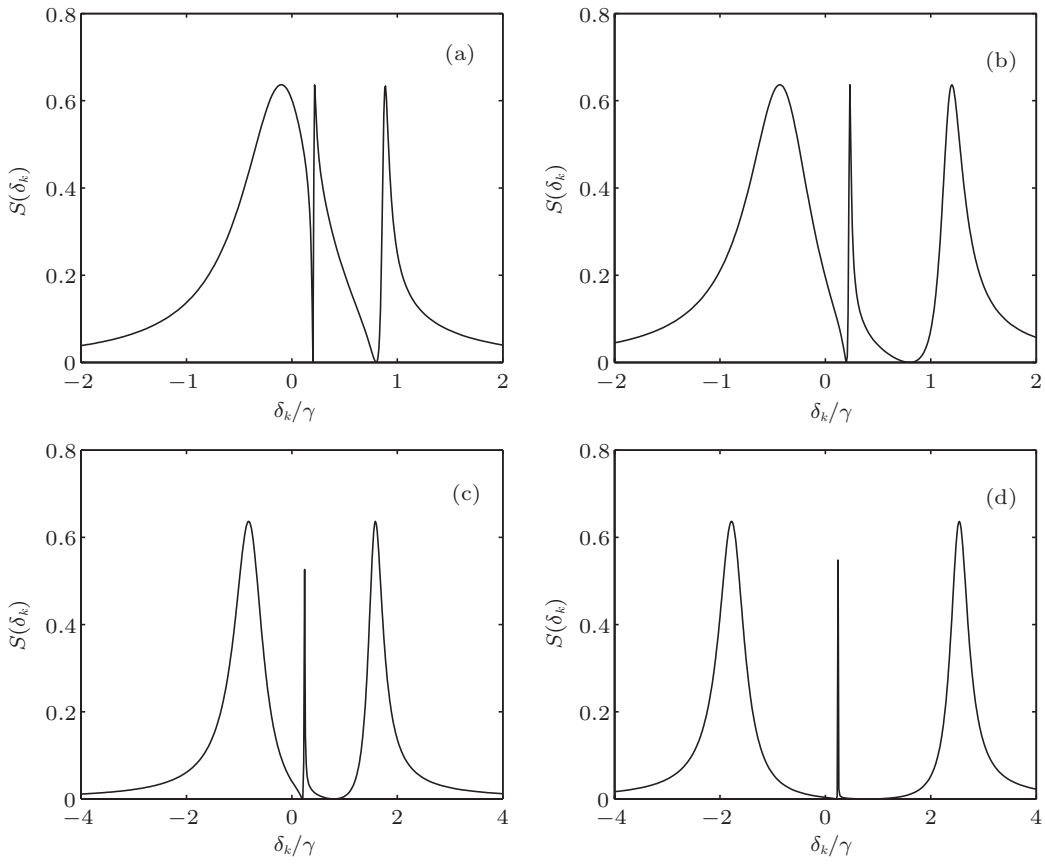


Fig. 4. Spontaneous emission spectra $S(\delta_k)$ (in units of γ^{-1}) for $\Delta_B = 0.3\gamma$, $\Delta_c = 0.5\gamma$, $\theta = \pi/6$, $a_3(0) = 1$, $a_1(0) = a_2(0) = 0$, and $\Gamma = \gamma$. (a) $\Omega_c = 0.2\gamma$; (b) $\Omega_c = 0.5\gamma$; (c) $\Omega_c = 0.8\gamma$; (d) $\Omega_c = 1.5\gamma$.

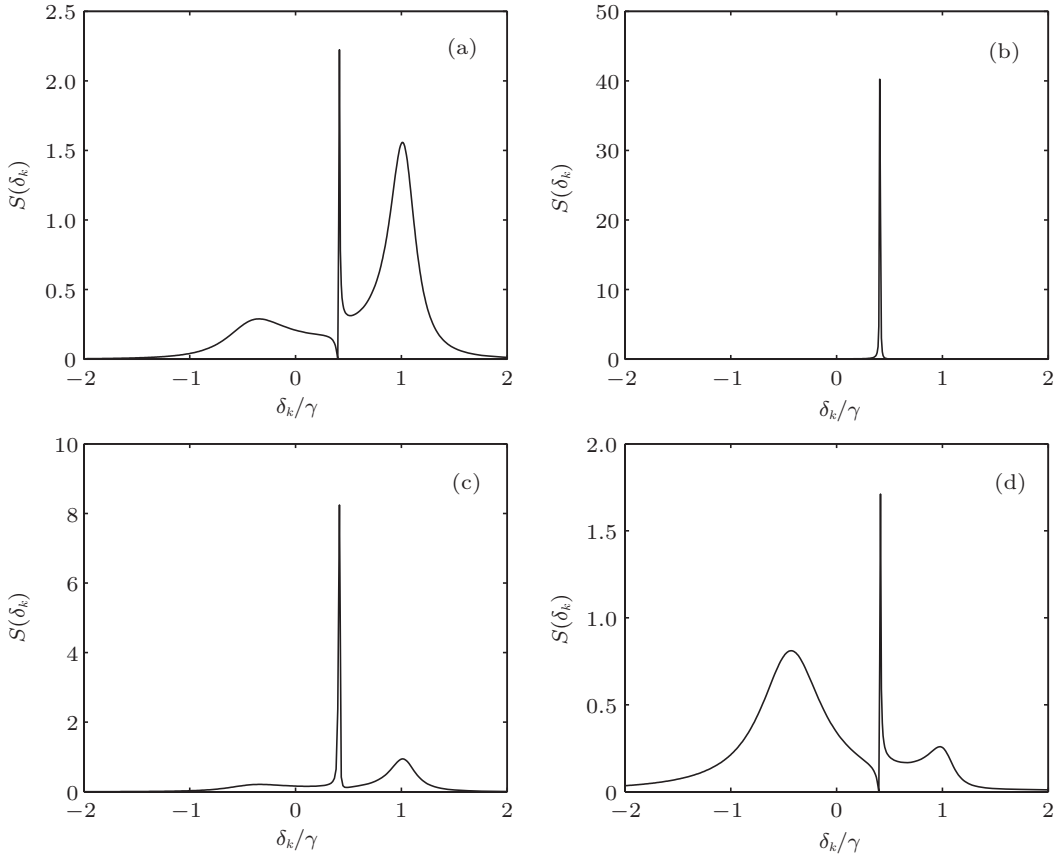


Fig. 5. Spontaneous emission spectra $S(\delta_k)$ (in units of γ^{-1}) for $\Delta_B = 0.1\gamma$, $\Delta_c = 0.5\gamma$, $\theta = \pi/6$, $\Omega_c = 0.5\gamma$, and $\Gamma = \gamma$. (a) $a_1(0) = 1$, $a_2(0) = a_3(0) = 0$; (b) $a_2(0) = 1$, $a_1(0) = a_3(0) = 0$; (c) $a_1(0) = a_2(0) = 1/\sqrt{2}$, $a_3(0) = 0$; (d) $a_1(0) = a_3(0) = 1/\sqrt{2}$, $a_2(0) = 0$.

$a_2(0) = a_3(0) = 0$, one fluorescence-quenching point exists in the spontaneous emission spectra, located at $\delta_k = 0.4\gamma$. Meanwhile, an ultranarrow spectral line at the fluorescence-quenching point $\delta_k = 0.4\gamma$ and two normal width sideband lines can be observed in Fig. 5(a). For the case that $a_2(0) = 1$ and $a_1(0) = a_3(0) = 0$, we can observe only one emission spectral line at $\delta_k = 0.4\gamma$ [see Fig. 5(b)]. For the case that $a_1(0) = a_2(0) = 1/\sqrt{2}$ and $a_3(0) = 0$, one ultranarrow central line and one normal width side line occur in the spontaneous emission spectra, while the left side line is greatly suppressed [see Fig. 5(c)]. When the initial probability amplitudes subject to $a_1(0) = a_3(0) = 1/\sqrt{2}$ and $a_2(0) = 0$, the emission spectra are similar to the case of $a_1(0) = 1$ and $a_2(0) = a_3(0) = 0$, and have an ultranarrow spectral line and two normal width side lines with one fluorescence-quenching point. However, we can find that the left side spectral line is enhanced obviously but the height of the right side spectral line becomes lower [see Fig. 5(d)].

4. Analysis in the dressed-state picture

In order to explicitly illustrate the NV center system under consideration, we will turn our attention to the dressed-state picture, generated by the two components of an elliptically polarized control field, namely, the $|1\rangle \leftrightarrow |3\rangle \leftrightarrow |2\rangle$ transitions together with the control field are treated as a coupled "NV center + field" system and the energy levels of the dressed states form a ladder of triplets, as shown in Fig. 1(b). In the dressed-state picture, the two components of an elliptically polarized control field, levels $|1\rangle$, $|2\rangle$, and $|3\rangle$ in the bare state can be replaced by three new states $|+\rangle$, $|0\rangle$, and $|-\rangle$. Such a subsystem is described by the interaction Hamiltonian

$$V = (\Delta_c + \Delta_B)|1\rangle\langle 1| + (\Delta_c - \Delta_B)|2\rangle\langle 2| + (\Omega_{c+}|3\rangle\langle 1| + \Omega_{c-}|3\rangle\langle 2| + \text{H.c.}).$$

After the mathematical calculation, we obtain the following equations for three dressed states and corresponding probability amplitudes:

$$|i\rangle = \cos\alpha\cos\beta|1\rangle + \cos\alpha\sin\beta|2\rangle + \sin\alpha|3\rangle, \quad (13)$$

$$a_i(t) = \cos\alpha\cos\beta a_1(t) + \cos\alpha\sin\beta a_2(t) + \sin\alpha a_3(t). \quad (14)$$

Here, $i = +, 0, -$,

$$\tan\alpha = \frac{\Omega_{c+}\Omega_{c-}}{\sqrt{(A\Omega_{c-})^2 + (B\Omega_{c+})^2}}, \quad \tan\beta = \frac{B\Omega_{c+}}{A\Omega_{c-}},$$

$$A = \lambda_i - \frac{|\Omega_{c-}|^2}{\lambda_i + \Delta_B - \Delta_c}, \quad B = \lambda_i - \frac{|\Omega_{c+}|^2}{\lambda_i - \Delta_B - \Delta_c},$$

with λ_i being the eigenvalue of level $|i\rangle$. From Eqs. (13) and (14), we can conclude that the ZPL spontaneous emission spectra should be generally composed of three peaks, which correspond to spontaneous emission $|i\rangle \rightarrow |4\rangle$ with $i = +, 0, -$, respectively. Multiple spontaneously generated coherence arises among these competitive transition pathways and results in spectral-line narrowing, spectra-line enhancement, spectral-line suppression, and fluorescence-quenching in the ZPL spontaneous emission spectra.

5. Possible experimental accessibility of the proposed scheme

Before ending this paper, let us briefly discuss the possible experimental realization of our proposed scheme of Fig. 1(a) by means of a single diamond NV center, an external magnetic field, and an elliptically polarized control field, which are described below respectively.

i) For NV centers, there is a relatively complicated structure of excited states, which includes six excited states.[44,65–67] The optical transitions in NV centers are spin-conserving. However, non-spin-conserving optical transitions occur in some cases because a set of excited states are highly sensitive to strain. Recent studies have suggested that, for a wide range of strain parameters, it is possible to obtain a Λ-type four-level system with multiple ground states coupled to a common excited state even at zero magnetic field due to factors such as strain which reduces the symmetry and primarily modifies the excited states.[47,48,68] The level diagram in Fig. 1(a) is appropriate for the strained case. The excited states are split by their orbital components into two spin triplets. As shown in Refs. [53] and [69] under strain, the non-spin-conserving transitions can be enhanced through the spin–orbit interaction. Alternatively, the individual excited state levels can be resolved at low temperature, as shown in Refs. [44] and [70].

Based on these facts, we consider, for instance, the NV center on the transitions $|3\rangle \leftrightarrow |^3A, m_s = 0\rangle$ or $|^3A, m_s = \pm 1\rangle$[37,44,48] as a possible candidate. A detailed coupling diagram and corresponding arrangements of experimental apparatus are shown in Fig. 1(a). Specifically, the designated states and the decay rates can be chosen as follows: the state $|3\rangle$ can be considered as a mixed state of two excited states $|A_2\rangle = (|E_-, m_s = +1\rangle + |E_+, m_s = -1\rangle)/\sqrt{2}$ and $|E_x\rangle = |X, m_s = 0\rangle$ under strain (i.e., $|3\rangle = \alpha|A_2\rangle + \beta|E_x\rangle$ with $|\alpha|^2 + |\beta|^2 = 1$), $|1\rangle = |^3A, m_s = -1\rangle$, $|2\rangle = |^3A, m_s = +1\rangle$, and $|4\rangle = |^3A, m_s = 0\rangle$, respectively. In the case of the NV center, however, we should pay attention to the decay rate $\gamma_{\text{total}} = 2\pi \times 13.4$ MHz[47,48] due to dipolar transitions. The spontaneous decay rate Γ within the ZPL range is only 3%–4% of γ_{total}.[53,68,71] In this case, the wavelength of an elliptically polarized control field is 637 nm, and the right(left)-circularly polarized component of an elliptically polarized control field is used to couple the transition $|3\rangle \leftrightarrow |1\rangle = |^3A, m_s = -1\rangle$ ($|3\rangle \leftrightarrow |2\rangle = |^3A, m_s = +1\rangle$).

ii) We briefly address the requirement of the magnetic field. We can employ an external magnetic field B along the quantized symmetry axis of the NV center to induce a Zeeman shift Δ_B. For example, when taking the Zeeman shift $\Delta_B = 1.5\gamma = 1.5\Gamma \simeq 1.5 \times 2\pi \times 0.4$ MHz in our numerical calculations, according to the relationship $2\Delta_B = \gamma_e B$ with the electron gyromagnetic ratio $\gamma_e = 2.8 \times 10^{10}$ Hz/T,[72] the magnetic field strength $B \simeq 1.8 \times 10^{-5}$ T = 18 Gs (1 Gs = 10^{-4} T) is needed and can be easily fulfilled in the experiment.

iii) The control field components Ω_{c+} and Ω_{c-} can be obtained through the following ways. Before applying to the NV center, the control beam passes through a half-wave plate followed by a quarter-wave plate.[54] The half-wave plate makes the control beam vertically polarized, and the quarter-wave plate has been rotated by an angle θ to control the polarization of the incoming vertically polarized control beam. After passing through the quarter-wave plate, the control beam becomes an elliptically polarized light which contains two components Ω_{c+} and Ω_{c-}.

6. Conclusion

In conclusion, we have theoretically explored the spontaneous emission spectra of the ZPL from a strained NV center system controlled by an elliptically polarized control field. The ellipticity of the control field is smoothly varied by means of a quarter-wave plate. The results clearly show that, by choosing appropriate parameters of the coupled system, such as Rabi frequency, the intensity of the external magnetic field, and initial population distribution, we can observe a very wide variety of spectral behavior ranging from an extremely enhanced ultranarrow spectral line to a depressed peak, from three peaks to double peaks, and different fluorescence-quenching points. In addition, the spectral behaviors are very sensitive to variables of the polarization-dependent phase difference of two components of the control field, so we can control the ZPL emission more conveniently. In the dressed-state picture, we demonstrated that this coherently driven NV center system has three close-lying levels and analyzed the spontaneous emission spectra resulting from multiple spontaneously generated coherence. Within the scope of the required experimental techniques, we briefly discussed the possible experimental realization of our proposed scheme. The research presented in this paper is useful in view of recent activity aiming at optical control of the NV centers.

Acknowledgments

We would like to thank professor Wu Ying for his encouragement and helpful discussions.

Appendix A: Derivation of the Hamiltonian (1)

In this Appendix A, we give a detailed derivation of the interaction Hamiltonian (1) involved in the main text. In the RWA and EDA, the whole Hamiltonian for the system under study in the Schrödinger's picture is given by

$$\hat{H} = \sum_{j=1}^{4} \hbar\omega_j |j\rangle\langle j| + \sum_k \hbar\omega_k b_k^\dagger b_k + \hbar\left(\Omega_{c+}\, e^{-i\omega_c t}|3\rangle\langle 1| + \Omega_{c-}\, e^{-i\omega_c t}|3\rangle\langle 2| + \sum_k g_k b_k |3\rangle\langle 4| + \text{H.c}\right), \quad \text{(A1)}$$

where $\hbar\omega_j$ is the energy of the state $|j\rangle$ ($j = 1$–4). Below we will take $\omega_1 = 0$ for the ground state $|1\rangle$ as the energy origin.

We can choose the proper free Hamiltonian as (with the assumption of $\hbar = 1$)

$$\hat{H}_0 = \omega_c|3\rangle\langle 3| + \omega_4|4\rangle\langle 4| + \sum_k \omega_k b_k^\dagger b_k. \quad \text{(A2)}$$

Then, turning into the interaction picture with respect to the above free Hamiltonian (A2) and using a unitary transformation

$$\begin{aligned} & U(t) \\ &= \exp\left(-i\hat{H}_0 t/\hbar\right) \\ &= \exp\left[-i\left(\omega_c|3\rangle\langle 3| + \omega_4|4\rangle\langle 4| + \sum_k \omega_k b_k^\dagger b_k\right)t\right], \end{aligned} \quad \text{(A3)}$$

we can derive the resulting effective Hamiltonian as follows:

$$\begin{aligned} \hat{H}_I &= U^\dagger(t)\hat{H}U(t) - iU^\dagger(t)\frac{\partial U(t)}{\partial t} \\ &= U^\dagger(t)\left(\hat{H} - \hat{H}_0\right)U(t) \\ &= 2\Delta_B|2\rangle\langle 2| + (\Delta_B + \Delta_c)|3\rangle\langle 3| \\ &\quad + \left[\Omega_{c+}|3\rangle\langle 1| + \Omega_{c-}|3\rangle\langle 2| \right. \\ &\quad \left. + \sum_k g_k b_k\, e^{-i(\Delta_B+\Delta_c-\delta_k)t}|3\rangle\langle 4| + \text{H.c.}\right]. \end{aligned} \quad \text{(A4)}$$

on the basis of the formula

$$\begin{aligned} & \exp\left(i\sum_n \omega_n|n\rangle\langle n|t\right)|j\rangle\langle k|\exp\left(-i\sum_n \omega_n|n\rangle\langle n|t\right) \\ &= |j\rangle\langle k|\exp\left(i\omega_j t - i\omega_k t\right). \end{aligned}$$

So the time factors of the third and fourth terms in Eq. (A1) are all eliminated in the interaction picture, which leads to the resulting Hamiltonian (1).

References

[1] Agarwal G S 1991 *Phys. Rev. Lett.* **67** 980
[2] Zibrov A S, Lukin M D, Nikonov D E, Hollberg L, Scully M O, Velichansky V L and Robinson H G 1995 *Phys. Rev. Lett.* **75** 1499
[3] Harris S E 1989 *Phys. Rev. Lett.* **62** 1033
[4] Gao J Y, Guo C, Guo X Z, Jin G X, Wang Q W, Zhao J, Zhang H Z, Jiang Y, Wang D Z and Jiang D M 1992 *Opt. Commun.* **93** 323
[5] Wu J H, Wang D P, Zhang H F, Xiao Z H and Gao J Y 2003 *Chin. Phys.* **12** 39
[6] Scully M O and Fleischhauer M 1992 *Phys. Rev. Lett.* **69** 1360
[7] Fleischhauer M, Matsko A B and Scully M O 2000 *Phys. Rev. A* **62** 013808
[8] Singh M R 2004 *Phys. Rev. A* **69** 023807
[9] Yang X X and Wu Y 2003 *Chin. Phys. Lett.* **20** 1736
[10] Scully M O 1991 *Phys. Rev. Lett.* **67** 1855
[11] Fleischhauer M, Keitel C H, Scully M O, Su C, Ulrich B T and Zhu S Y 1992 *Phys. Rev. A* **46** 1468
[12] Wang F, Gong C, Tan X Y and Shi W X 2012 *Chin. Phys. B* **21** 114206
[13] Bennett C H and Divincenzo D P 2000 *Nature* **404** 247
[14] Petrosyan D and Malakyan Y P 2004 *Phys. Rev. A* **70** 023822
[15] Paternostro M, Kim M S and Knight P L 2005 *Phys. Rev. A* **71** 022311
[16] Jiang X Q, Zhang B, Lu Z W and Sun X D 2011 *Phys. Rev. A* **83** 053823
[17] Li G X, Evers J and Keitel C H 2009 *Phys. Rev. B* **80** 045102
[18] Zeng X D, Li G X, Yang Y P and Zhu S Y 2012 *Phys. Rev. A* **86** 033819
[19] Singh M R 2007 *Phys. Rev. A* **75** 033810
[20] Singh M R 2006 *J. Phys. B: At. Mol. Opt. Phys.* **39** 5131
[21] Singh M R 2007 *Phys. Lett. A* **363** 177
[22] Angelakis D G, Paspalakis E and Knight P L 2001 *Phys. Rev. A* **64** 013801
[23] Yang Y, Fleischhauer M and Zhu S Y 2003 *Phys. Rev. A* **68** 043805
[24] Agarwal G S and Pathak P K 2004 *Phys. Rev. A* **70** 025802
[25] Tan R and Li G X 2005 *Acta Phys. Sin.* **54** 2059 (in Chinese)
[26] Huang X S, Liu H L and Wang D 2012 *Chin. Phys. B* **21** 054218
[27] Zhu S Y and Scully M O 1996 *Phys. Rev. Lett.* **76** 388
[28] Paspalakis E and Knight P L 1998 *Phys. Rev. Lett.* **81** 293
[29] Paspalakis E, Keitel C H and Knight P L 1998 *Phys. Rev. A* **58** 4868
[30] Gu W J and Li G X 2012 *Phys. Rev. A* **85** 014101
[31] Wu J H, Li A J, Ding Y, Zhao Y C and Gao J Y 2005 *Phys. Rev. A* **72** 023802
[32] Li A J, Song X L, Wei X G, Wang L and Gao J Y 2008 *Phys. Rev. A* **77** 053806
[33] Qi J B 2009 *Phys. Rev. A* **80** 043827
[34] Jelezko F, Gaebel T, Popa I, Domhan M, Gruber A and Wrachtrup J 2004 *Phys. Rev. Lett.* **93** 130501
[35] Epstein R J, Mendoza F M, Kato Y K and Awschalom D D 2005 *Nat. Phys.* **1** 94
[36] Gaebel T, Domhan M, Popa I, Wittmann C, Neumann P, Jelezko F, Rabeau J R, Stavrias N, Greentree A D, Prawer S, Meijer J, Twamley J, Hemmer P R and Wrachtrup J 2006 *Nat. Phys.* **2** 408
[37] Dutt M V G, Childress L, Jiang L, Togan E, Maze J, Jelezko F, Zibrov A S, Hemmer P R and Lukin M D 2007 *Science* **316** 1312
[38] Hanson R, Dobrovitski V V, Feiguin A E, Gywat O and Awschalom D D 2008 *Science* **320** 352
[39] Park Y S, Cook A K and Wang H 2006 *Nano Lett.* **6** 2075
[40] Larsson M, Dinyari K N and Wang H 2009 *Nano Lett.* **9** 1447
[41] van der Sar T, Wang Z H, Blok M S, Bernien H, Taminiau T H, Toyli D M, Lidar D A, Awschalom D D, Hanson R and Dobrovitski V V 2012 *Nature* **484** 82
[42] de Lange G, Wang Z H, Riste D, Dobrovitski V V and Hanson R 2010 *Science* **330** 60
[43] Fuchs G D, Falk A L, Dobrovitski V V and Awschalom D D 2012 *Phys. Rev. Lett.* **108** 157602
[44] Togan E, Chu Y, Trifonov A S, Jiang L, Maze J, Childress L, Dutt M V G, Sørensen A S, Hemmer P R, Zibrov A S and Lukin M D 2010 *Nature* **466** 730
[45] Yang W L, Yin Z Q, Chen Z X, Kou S P, Feng M and Oh C H 2012 *Phys. Rev. A* **86** 012307
[46] Yang W L, Yin Z Q, Xu Z Y, Feng M and Du J F 2010 *Appl. Phys. Lett.* **96** 241113

[47] Santori C, Barclay P E, Fu K M C, Beausoleil R G, Spillane S and Fisch M 2010 *Nanotechnology* **21** 274008

[48] Santori C, Tamarat P, Neumann P, Wrachtrup J, Fattal D, Beausoleil R G, Rabeau J, Olivero P, Greentree A D, Prawer S, Jelezko F and Hemmer P 2006 *Phys. Rev. Lett.* **97** 247401

[49] Yang W L, Yin Z Q, Xu Z Y, Feng M and Oh C H 2011 *Phys. Rev. A* **84** 043849

[50] Yang W L, An J H, Zhang C, Feng M and Oh C H 2013 *Phys. Rev. A* **87** 022312

[51] Wang Z H and Dobrovitski V V 2011 *Phys. Rev. B* **84** 045303

[52] Wolters J, Schell A W, Kewes G, Nüsse N, Schoengen M, Döscher H, Hannappel T, Löchel B, Barth M and Benson O 2010 *Appl. Phys. Lett.* **97** 141108

[53] Manson N B, Harrison J P and Sellars M J 2006 *Phys. Rev. B* **74** 104303

[54] Khadka U, Zhang Y P and Xiao M 2010 *Phys. Rev. A* **81** 023830

[55] Singh M R 2009 *Opt. Lett.* **34** 2909

[56] Wu Y and Yang X X 2004 *Phys. Rev. A* **70** 053818

[57] Wu Y and Yang X X 2005 *Phys. Rev. A* **71** 053806

[58] Wu Y, Payne M G, Hagley E W and Deng L 2004 *Phys. Rev. A* **69** 063803

[59] Petrosyan D and Kurizki G 2001 *Phys. Rev. A* **64** 023810

[60] Singh M R and Lipson R H 2008 *J. Phys. B: At. Mol. Opt. Phys.* **41** 015401

[61] Xia H R, Ye C Y and Zhu S Y 1996 *Phys. Rev. Lett.* **77** 1032

[62] Liu C P, Gong S Q, Fan X J, Jin S Q and Xu Z Z 2006 *Opt. Commun.* **254** 368

[63] Liu C P, Gong S Q, Fan X J and Xu Z Z 2004 *Opt. Commun.* **231** 289

[64] Liu C P, Gong S Q, Fan X J and Xu Z Z 2004 *Opt. Commun.* **239** 383

[65] Batalov A, Jacques V, Kaiser F, Siyushev P, Neumann P, Rogers L J, McMurtrie R L, Manson N B, Jelezko F and Wrachtrup J 2009 *Phys. Rev. Lett.* **102** 195506

[66] Tamarat P, Manson N B, Harrison J P, McMurtrie R L, Nizovtsev A, Santori C, Beausoleil R G, Neumann P, Gaebel T, Jelezko F, Hemmer P and Wrachtrup J 2008 *New J. Phys.* **10** 045004

[67] Neumann P, Kolesov R, Jacques V, Beck J, Tisler J, Batalov A, Rogers L, Manson N B, Balasubramanian G, Jelezko F and Wrachtrup J 2009 *New J. Phys.* **11** 013017

[68] Santori C, Fattal D, Spillane S M, Fiorentino M, Beausoleil R G, Greentree A D, Olivero P, Draganski M, Rabeau J R, Reichart P, Gibson B C, Rubanov S, Jamieson D N and Prawer S 2006 *Opt. Express* **14** 7986

[69] Maze J R, Gali A, Togan E, Chu Y, Trifonov A, Kaxiras E and Lukin M D 2011 *New J. Phys.* **13** 025025

[70] Aharonovich I, Castelletto S, Simpson D A, Su C H, Greentree A D and Prawer S 2011 *Rep. Prog. Phys.* **74** 076501

[71] Fuchs G D, Dobrovitski V V, Hanson R, Batra A, Weis C D, Schenkel T and Awschalom D D 2008 *Phys. Rev. Lett.* **101** 117601

[72] Ofori-Okai B K, Pezzagna S, Chang K, Loretz M, Schirhagl R, Tao Y, Moores B A, Groot-Berning K, Meijer J and Degen C L 2012 *Phys. Rev. B* **86** 081406(R)